

Investigation of Ferritic Superalloys by Computational Design and Experimental Validation

Investigators: Mark D. Asta², Gautam Ghosh³, David C. Dunand³, Morris E. Fine³,
Chain T. Liu⁴, and Peter K. Liaw¹

Ph.D. Students: Hong Ding², Sharon Huang¹, Michael Rawings³,
Gian Song¹, Zhiqian Sun¹, and Kevin Teng¹

Research Associates: Gongyao Wang¹, Nhon Q Vo³, and Christian Liebscher²

1. Department of Materials Science and Engineering, The University of Tennessee (UT), Knoxville, TN 37996, USA
2. Department of Materials Science and Engineering, University of California (UC), Berkeley, CA 94720, USA
3. Department of Materials Science and Engineering, Northwestern University (NU), Evanston, IL 60208-3108, USA
4. Systems Engineering and Engineering Management and Mechanical and Biomedical Engineering, City University of Hong Kong, Hong Kong

Acknowledgements

We are very grateful to:

- (1) Richard Dunst
- (2) Vito Cedro
- (3) Patricia Rawls
- (4) Robert Romanosky
- (5) Susan Maley
- (6) Conrad Regis
- (7) Nicholas Anderson, for their kind support and encouragement, and
- (8) National Energy Technology Laboratory (NETL) for sponsoring this project

Outline

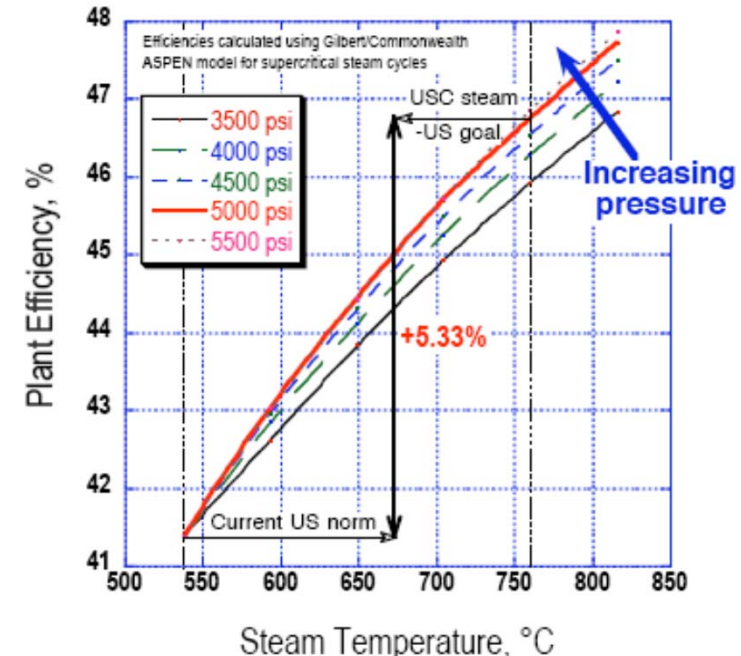
- ❖ Introduction – Why NiAl/Ni₂TiAl-strengthened ferritic steels
- ❖ Objectives
- ❖ First-Principles Calculations
 - ❖ Calculations of Interfacial Energies for Fe, *B2*, and *L2₁* Phases
- ❖ Coarsening Kinetics of NiAl Precipitates
- ❖ NiAl/Ni₂TiAl-Strengthened Ferritic Superalloys (Transmission Electron Microscopy and Creep Behavior)
- ❖ In-situ Neutron Creep Studies
- ❖ Dislocation-Dynamics Simulations
- ❖ Papers and Presentations
- ❖ Future Work
- ❖ Conclusions

1. Introduction

Ferritic alloys as candidates for fossil-energy power plants

Why ferritic steels? Why not Ni-based alloys?

- 80% of all electricity generation in the world is produced using steam turbines. Thus, low-cost materials are required.
- The materials with good thermal conductivity, low density and low thermal expansion are preferable for thick-section components of the steam turbine.



P. Maziasz, I. Wright, J. Shingledecker, T. Gibbons, R. Romanosky, *Proceedings from the fourth international conference on advances for materials technology for fossil power plants 2005*

Properties Materials	Thermal Expansion Coefficient [2]	Thermal Conductivity [3]	Density [4]	Cost (\$/t) [5]
Ferritic Steels	$1.0 \times 10^{-5} \text{ K}^{-1}$	50 W/(m·K)	7.85 g/cm ³	< \$900
Ni-based Superalloys	$1.8 \times 10^{-5} \text{ K}^{-1}$	21 W/(m·K)	8.97 g/cm ³	> \$40K

[1] http://en.wikipedia.org/wiki/Steam_turbine

[2] <http://www.handyharmancanada.com/TheBrazingBook/comparis.htm>

[3] http://en.wikipedia.org/wiki/List_of_thermal_conductivities

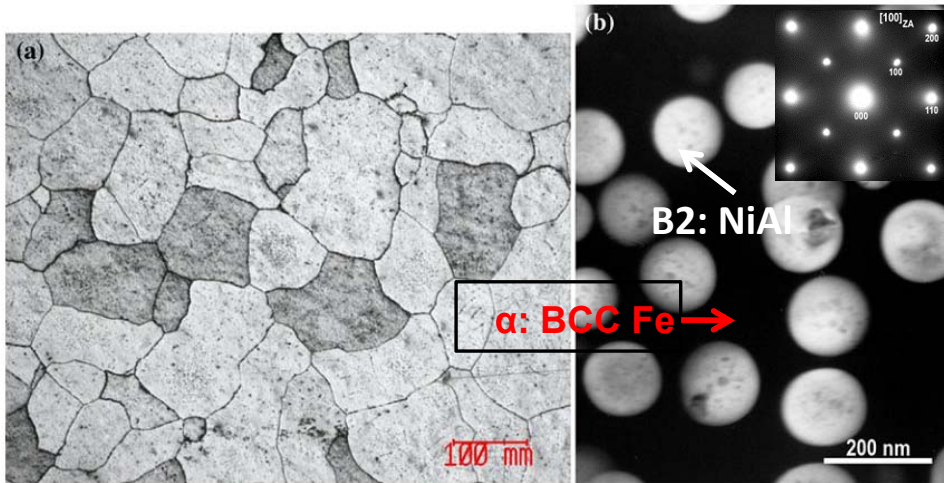
[4] Z. Sun, C.H. Liebscher, S. Huang, Z. Teng, G. Song, G. Wang, M. Asta, M. Rawlings, M.E. Fine, and P.K. Liaw, *Scripta Materialia* 68 (2013) 384

[5] http://www.ttiinc.com/page/ME_Materials

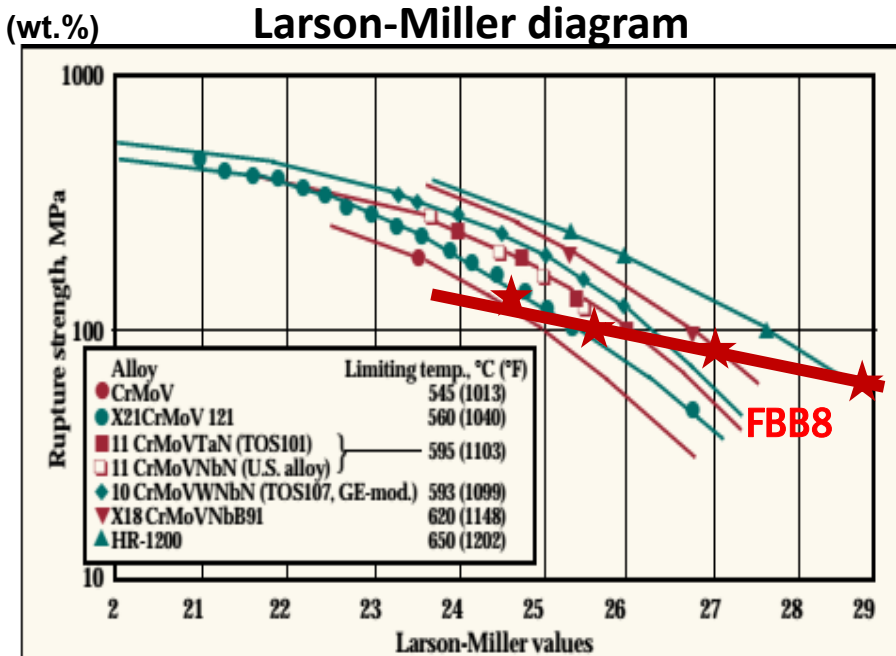
1. Introduction

Critical issues to address on NiAl-strengthened ferritic alloys

FBB8: Fe-6.5Al-10Cr-10Ni-3.4Mo-0.25Zr-0.005B, weight percent (wt.%)



S. Huang, D. Brown, B. Clausen, Z. Teng, Y. Gao. P. Liaw. (2011). Metallurgical and Materials Transactions A, 43, pp. 1497-1508



$$L = T \times (C + \log t_h)/1000$$

R. Viswanathan. (2004). Advanced Materials & Processes, vol. 162, pp. 73-76

At Low stresses (< 100 MPa) → higher or comparable creep resistance

However....

At high stresses (> 100 MPa) → inferior creep resistance compared to other Fe-based materials candidates for steam-turbine applications

$$L = T \times (C + \log t_h)/1000$$

L : Larson-Miller parameter

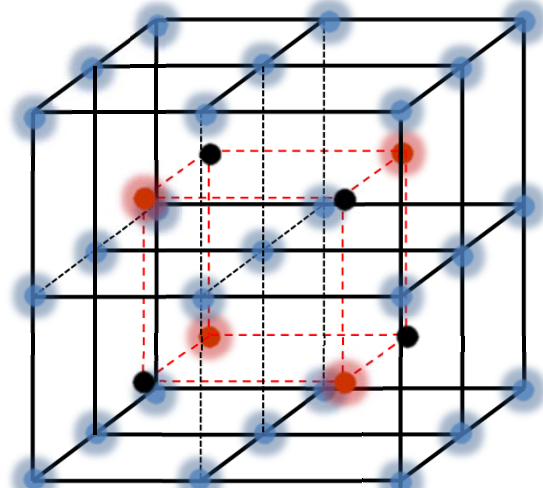
T : Temperature in Kelvin

C : Larson-Miller constant

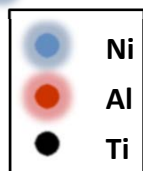
t_h : Time in hour

1. Introduction

Structural similarity of NiAl and Ni_2TiAl phases

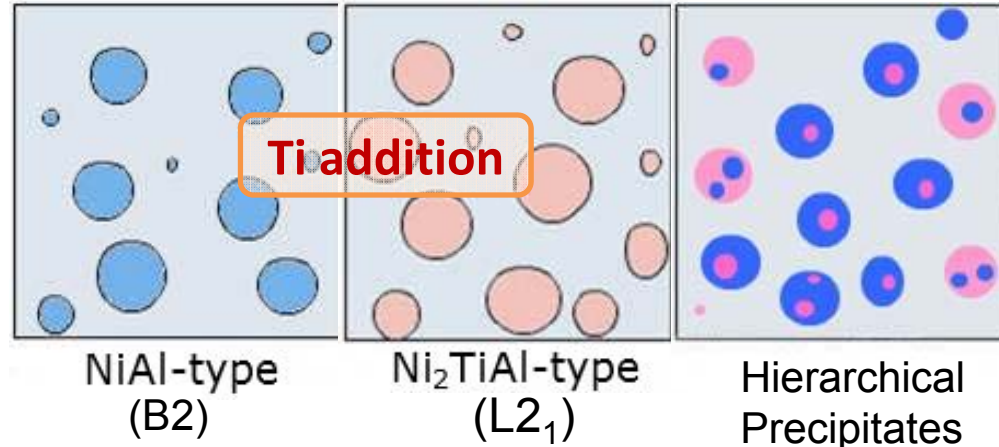


Ni_2TiAl ($\text{L}2_1$)
 $a = 0.5865 \text{ nm}$



The small cells constituting the large Ni_2AlTi unit cell are 1.7 % larger in size than the NiAl unit cell

P. R. Strutt, R. S. Polvani, and J. C. Ingram.
Metallurgical Transaction A. 7, 23 (1976)
R. S. Polvani, W. S. Tzeng, and P. R. Strutt.
Metallurgical Transaction A. 7, 33 (1976)



- The elevated-temperature strength of NiAl-type (B2) precipitates is limited by their properties.
- The creep strength (defined as the stress to maintain a steady-state rate of 10^{-7} s^{-1}) of Ni_2TiAl ($\text{L}2_1$) between 1,026 to 1,273 K is about three times that of NiAl in its most creep-resistant form.
- The creep strength of NiAl- Ni_2TiAl two-phase alloys are more creep resistant than either of the phases in its monolithic form and at least comparable to the Ni-based superalloy, MAR-M200 (nominal composition wt.-%: Cr 9.0; Co 10.0; W 12.5; Nb 1.0; Ti 2.0; Al 5.0; C 0.15; B 0.015; Ni balance).

2. Objectives

- **Objective 1:** To develop and integrate modern computational tools and algorithms required to assist in the optimization of creep properties of high-temperature alloys for fossil-energy applications
- **Objective 2:** To achieve fundamental understanding of the processing-microstructure-property-performance links underlying the creep behavior of novel ferritic superalloys strengthened by *B2 and/or L2₁* intermetallics.

3 Calculations of Interfacial Energies for Fe, B2, and L2₁ Phases

- Sharp Interface Models
 - Construction of structural models (supercells) followed by total energy calculation from first principles
- Diffuse Interface Models
 - Cluster expansion followed by Monte Carlo simulation
 - In progress
- Supercell Method (Sharp Interface):
 - Supercells of different sizes are constructed with {100}, {110} and {111} habits. Supercells are gradually increased in a direction perpendicular to the habit plane
 - Convergence of calculated interfacial energy is checked w.r.t. the supercell size
 - Calculated Fe/L2₁ interfacial energy (γ) is defined as

$$\gamma = (E_{Fe/L2_1}[n_{Fe}, n_{L2_1}] - 0.5(E_{Fe}[2n_{Fe}] + E_{L2_1}[2n_{L2_1}])) / 2A$$

n_{Fe} and n_{L2_1} : Numbers of unit cells of Fe and L2₁ phases, respectively.

E : Corresponding total energy;

A : Interfacial area.

Similarly, B2/L2₁ interfacial energy may be defined.

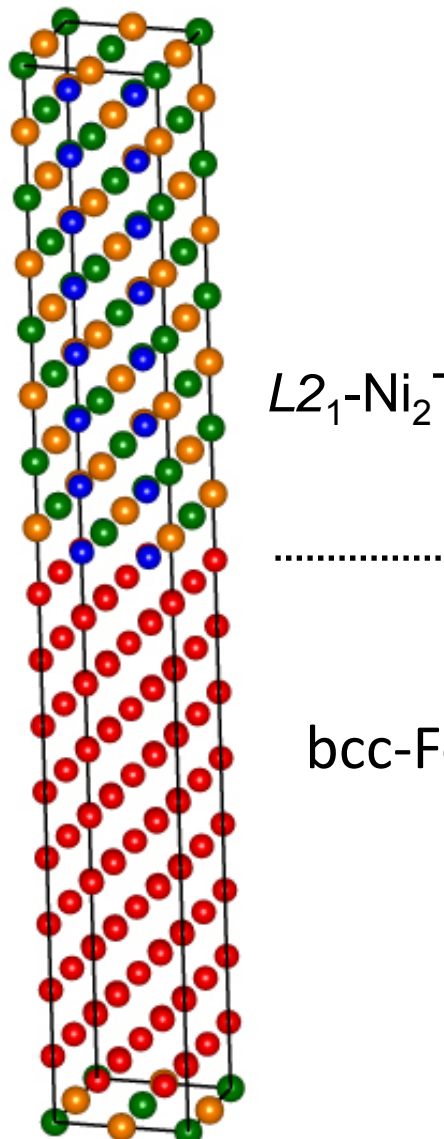
3 Calculations of Interfacial Energies for Fe, $B2$, and $L2_1$ Phases

- Three distinct coherent interfaces
 - bcc-Fe/ $B2$ -NiAl
 - bcc-Fe/ $L2_1$ - Ni_2TiAl
 - $B2$ -NiAl/ $L2_1$ - Ni_2TiAl
- Historically, the interfacial energy in two-phase microstructures has been “derived” by employing coarsening (Oswald ripening) theory
 - However, it is time (resource) consuming: may require multiple expt. techniques (e.g., TEM, X-ray, neutron, etc.)
 - An alternative viable option is to calculate from first principles
- Enormous resources are needed to experimentally determine three types of interfacial energies
- As a part of this research, we have calculated the interfacial energies from first principles.

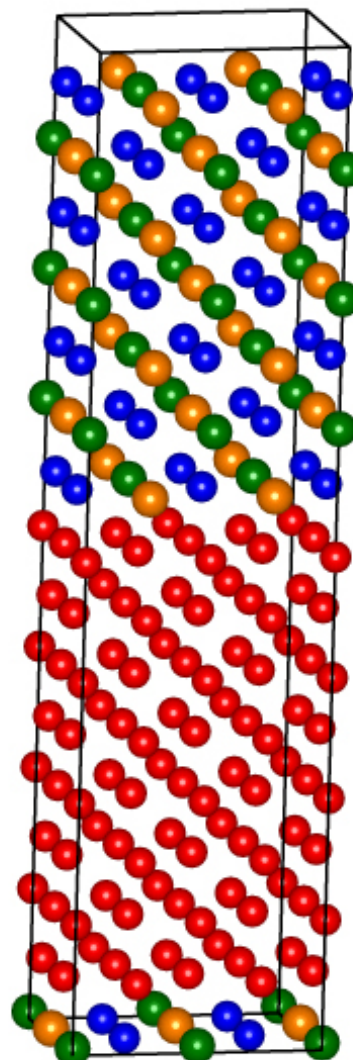
3 Calculations of Interfacial Energies for Fe, B2, and L2₁ Phases

Atomic scale structural models of bcc-Fe/L2₁-Ni₂TiAl with a coherent interface:

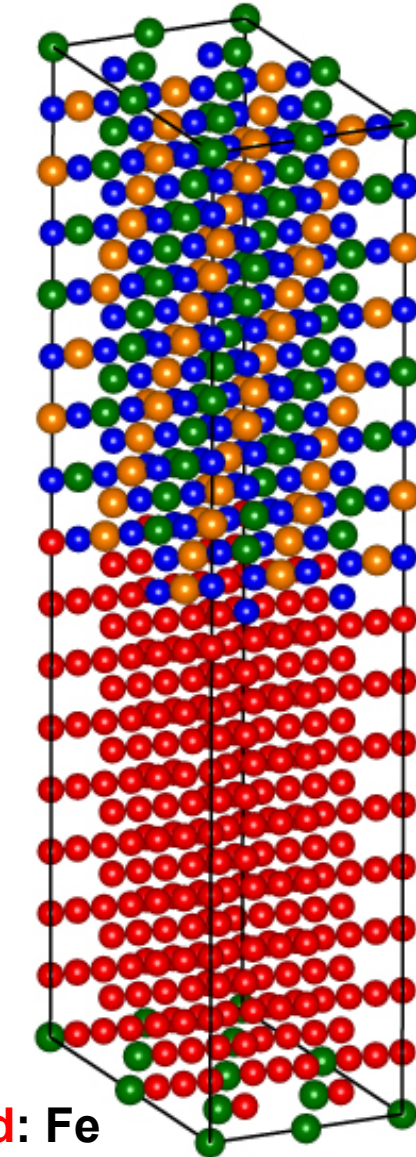
(100) habit



(110) habit



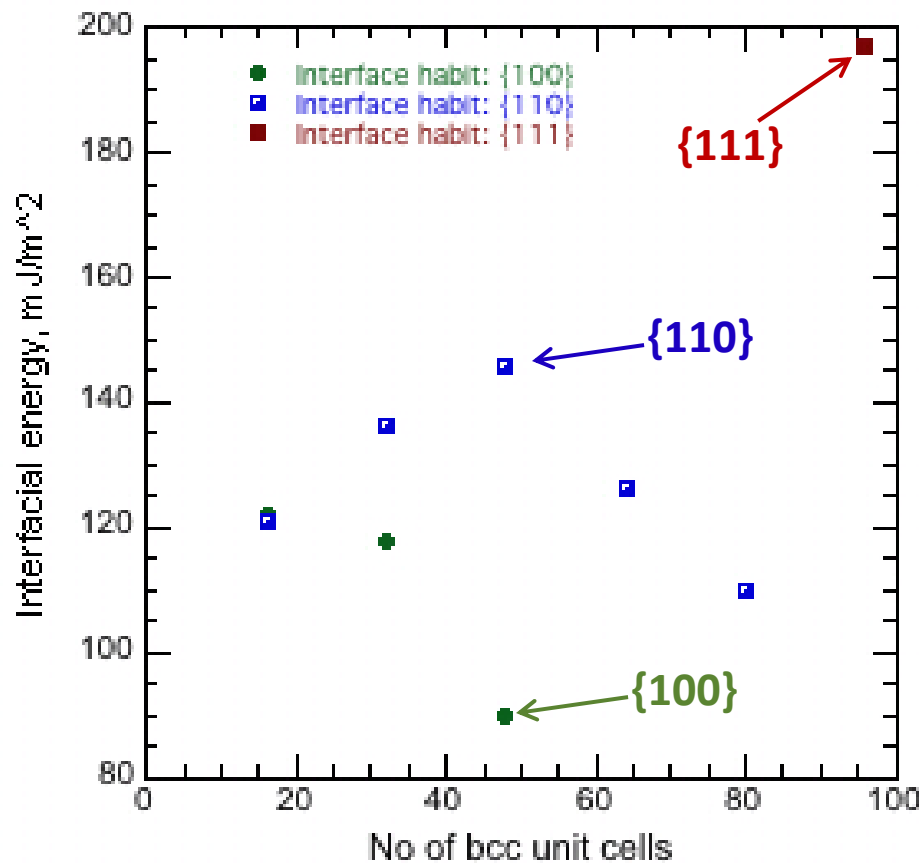
(111) habit



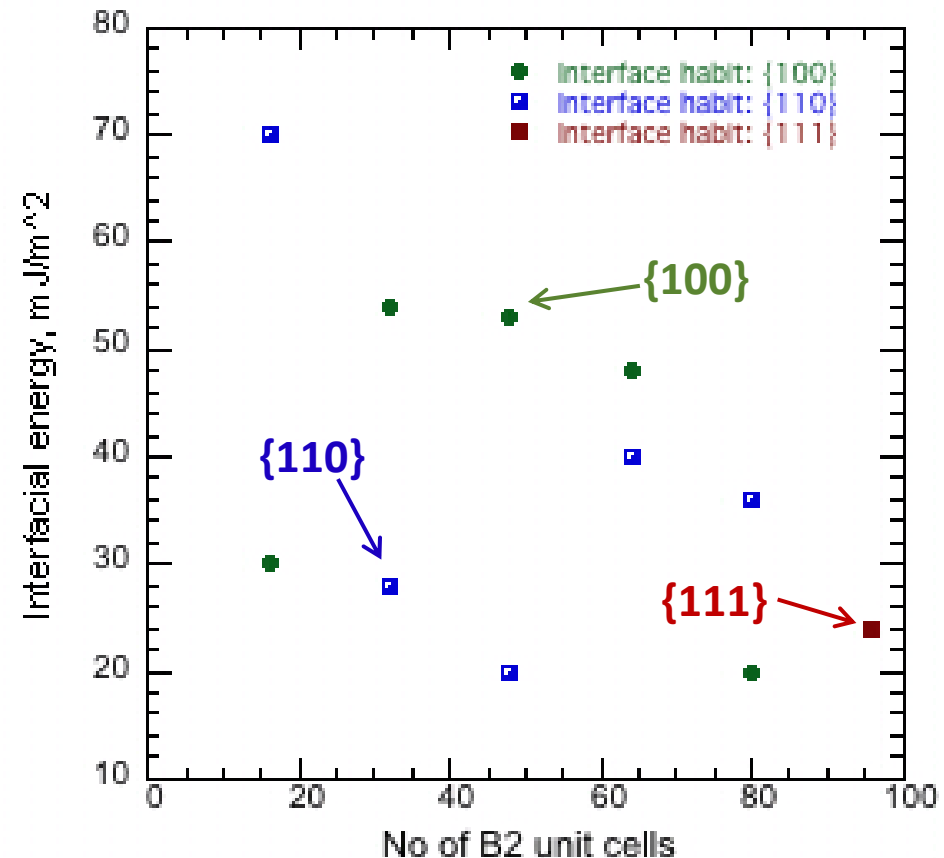
green: Ni, blue: Al, yellow: Ti, red: Fe

3 Calculation of Interfacial Energies for Fe, B2, and L2₁ Phases

bcc-Fe/L2₁-Ni₂TiAl



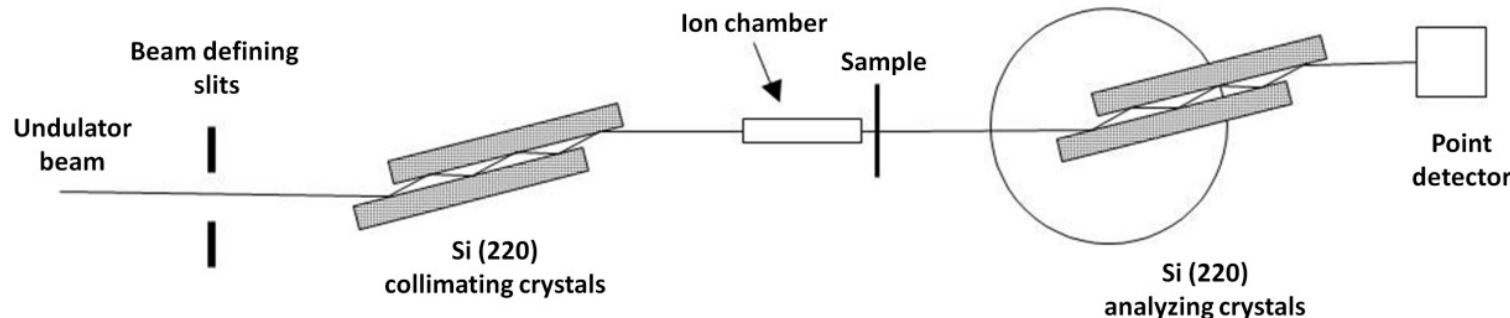
B2-NiAl/L2₁-Ni₂TiAl



- In progress: Calculations involving larger supercells
- It's obvious that for any habit, the coherent interfacial energy of NiAl/Ni₂TiAl << Fe/Ni₂TiAl

4 Coarsening Kinetics of NiAl Precipitates in FBB8

Ultra-Small-Angle X-ray Scattering (USAXS), Beamline 15-ID-D, at Advanced Photon Source, Argonne National Laboratory:



The scattering intensity can be described as

$$I(\mathbf{q}) = nF(\mathbf{q}, \mathbf{r})S(\mathbf{q})$$

\mathbf{q} : Scattering vector and defined as $\frac{4\pi}{\lambda} \sin \theta$ (λ is the X-ray wavelength, and θ is the angle between the incident and scattered wave vectors);

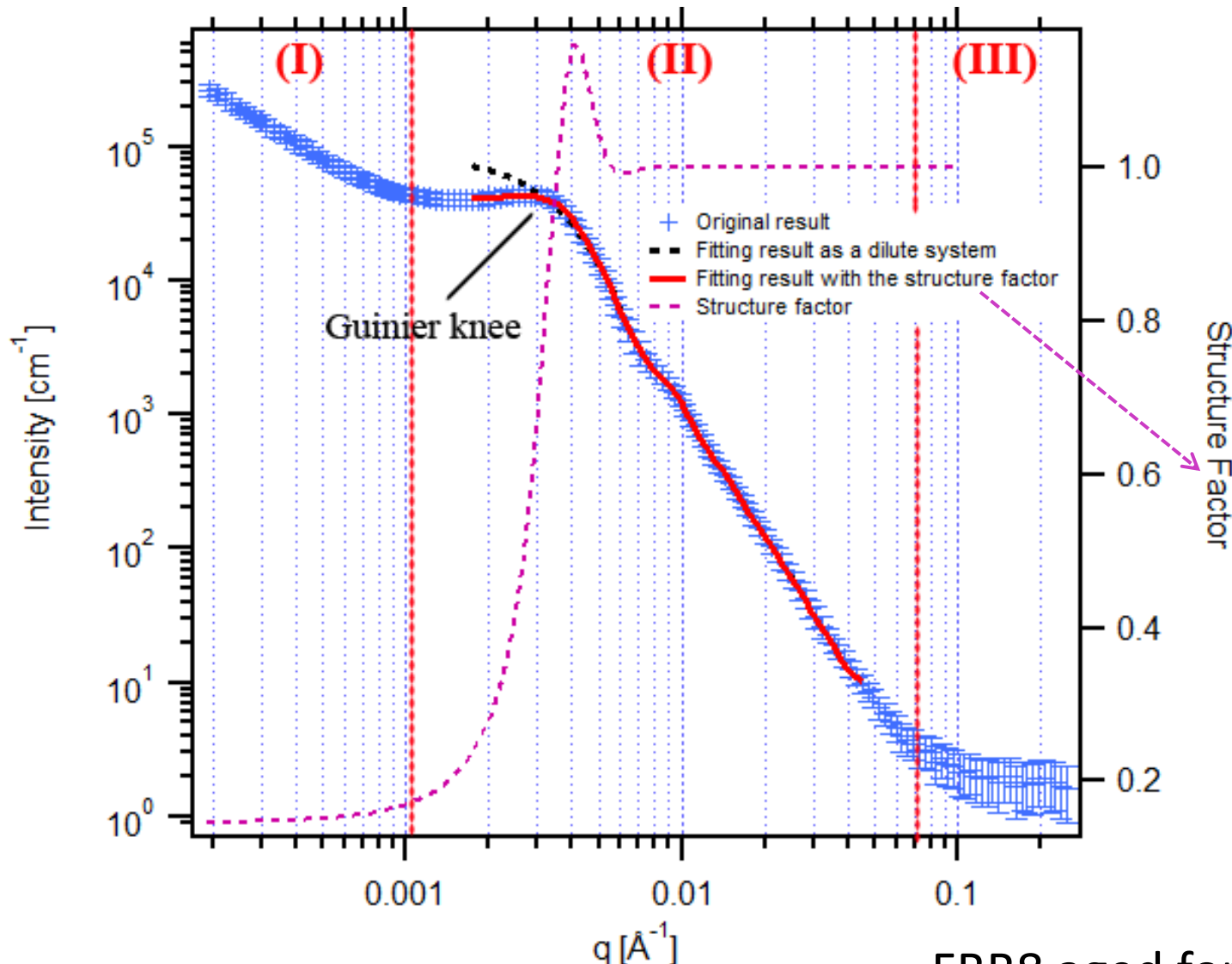
$$F(\mathbf{q}, \mathbf{r}) = \Delta\rho 4\pi r^3 \frac{\sin qr - qr \cos qr}{(qr)^3}$$

n : Total number of particles;
 \mathbf{r} : Particle size;
 F : Form factor;
 S : Structure factor.

$$S(\mathbf{q}) = 2 \frac{1 - e^{-q^2 \sigma^2 / 4} \cos(qL)}{1 - 2e^{-q^2 \sigma^2 / 4} \cos(qL) + e^{-q^2 \sigma^2 / 2}} - 1$$

$\Delta\rho(r)$: Contrast between particles and the matrix; L : Inter-precipitate distance; σ : Standard deviation of L

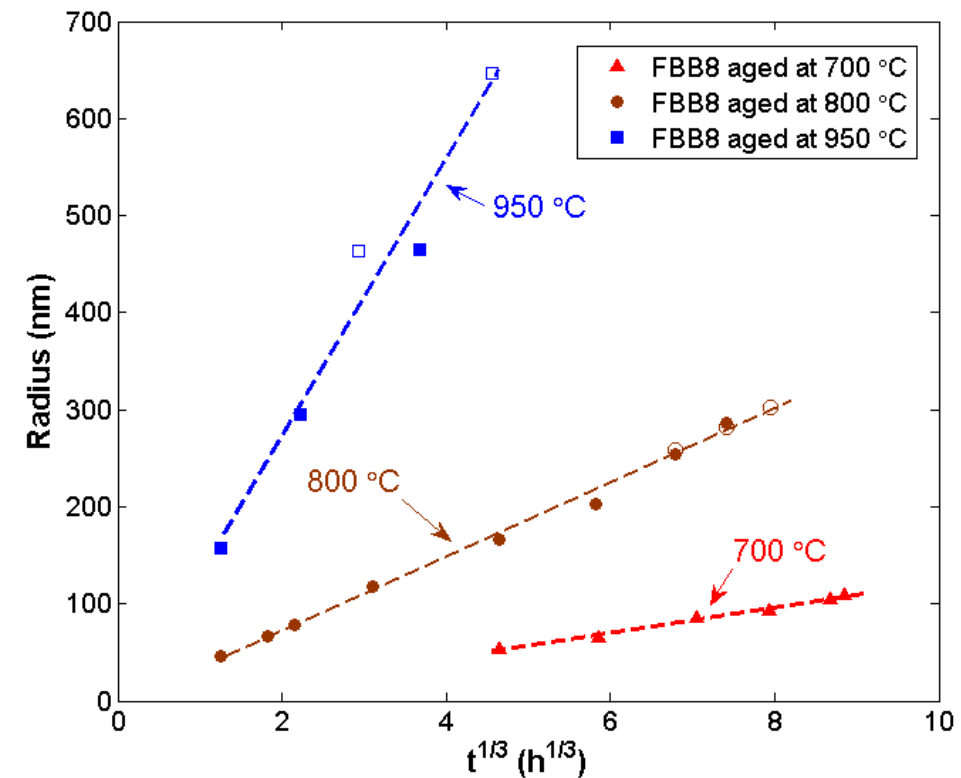
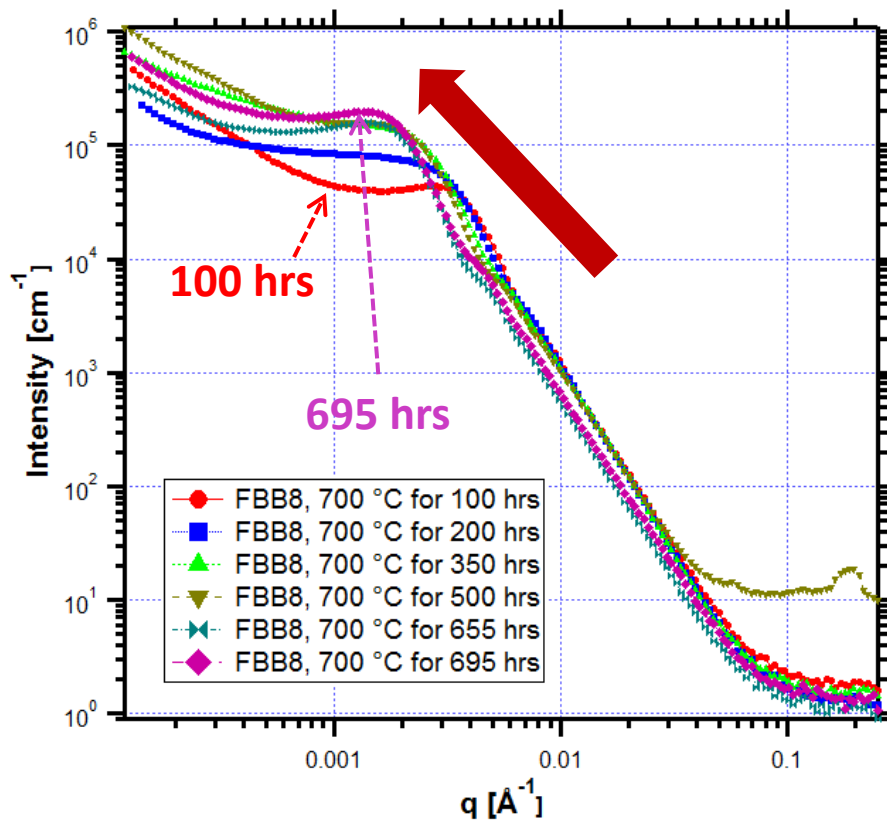
4 Coarsening Kinetics of NiAl Precipitates in FBB8



- I: The feature may come from the grain structure and segregation.
- II: The feature comes from precipitates.
- III: There is the background interference

FBB8 aged for 100 hours at 700 °C:
 $\bar{r} = 54 \text{ nm}$.

4 Coarsening Kinetics of NiAl Precipitates in FBB8



the coarsening kinetics of NiAl precipitates in the α -iron matrix satisfies the Lifshitz-Slyozov-Wagner (LSW) theory

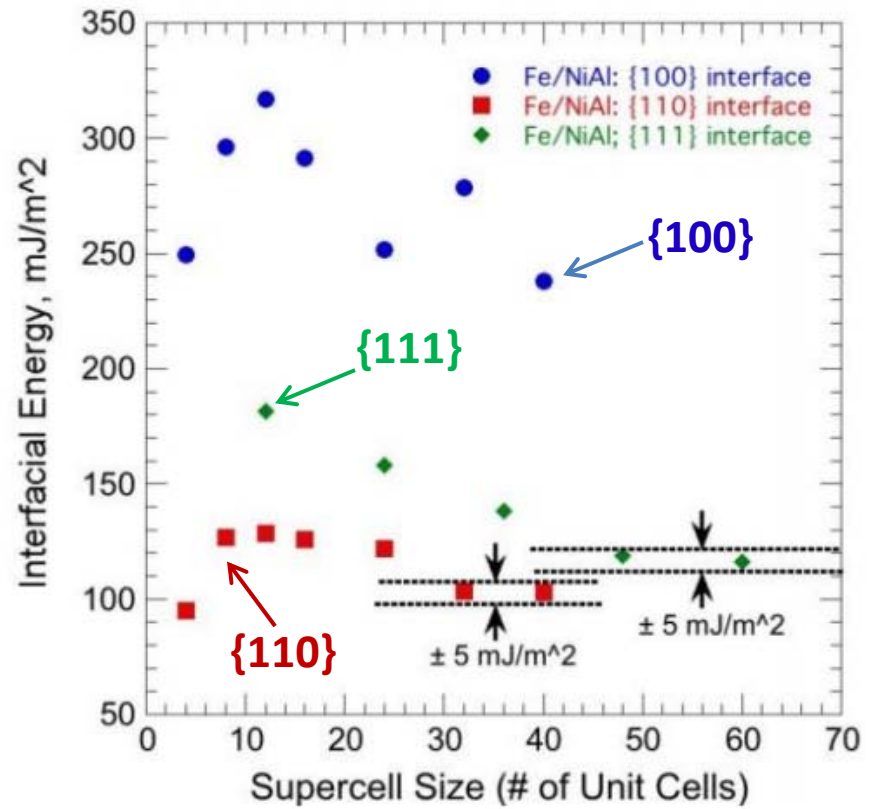
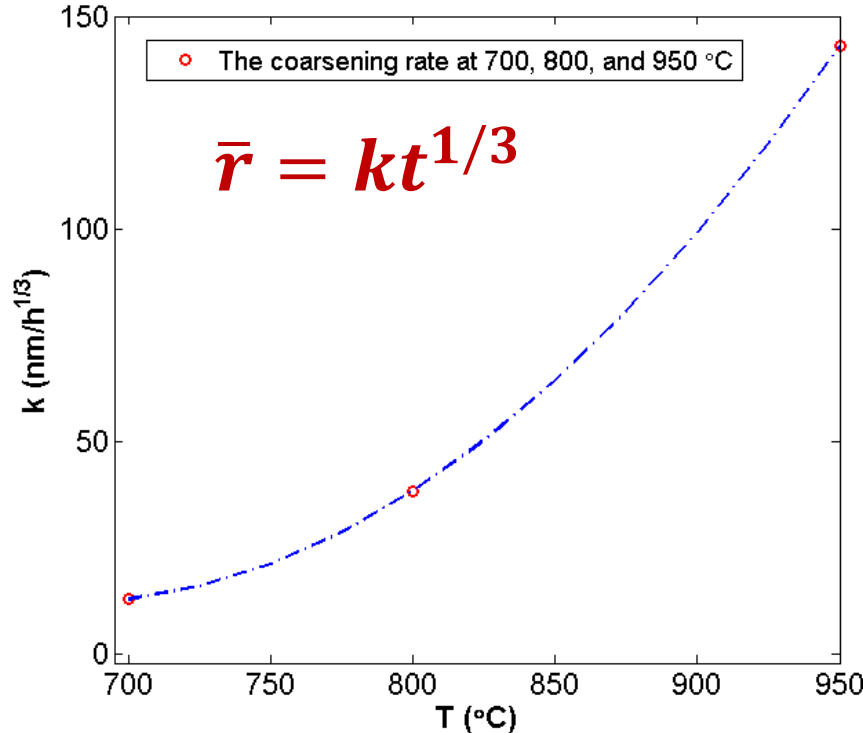
$$\bar{r} = kt^{1/3}$$

k: Coarsening rate;

t: Aging time.

	700 °C	800 °C	950 °C
k (nm/h ^{1/3})	13	38	143

4 Coarsening Kinetics of NiAl Precipitates in FBB8



The cubic of the coarsening rate, k , can be expressed as

$$k^3 \sim \frac{8V_m^{NiAl}\gamma}{9RT \sum_{i=2}^N (\bar{C}_i^{NiAl} - \bar{C}_i^{\alpha\text{-iron}})^2 / D_i \bar{C}_i^{\alpha\text{-iron}}}$$

V_m^{NiAl} : Molar volume of NiAl precipitates; γ : Interfacial energy between NiAl precipitates and the α -iron matrix; D : Effective diffusion coefficient of element i ; \bar{C}_i^{NiAl} and $\bar{C}_i^{\alpha\text{-iron}}$: Equilibrium mole fractions of the component i in NiAl precipitates and the α -iron matrix, respectively; R : Gas constant; T : Temperature.

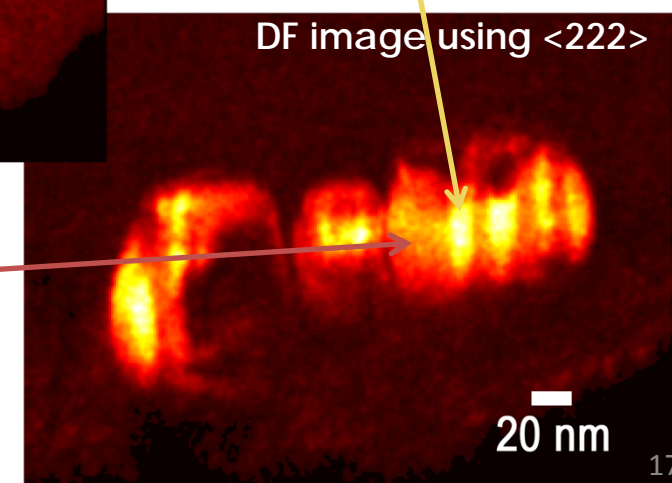
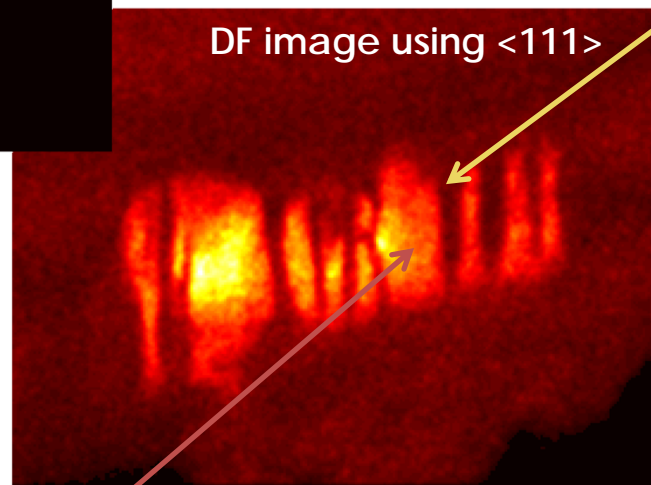
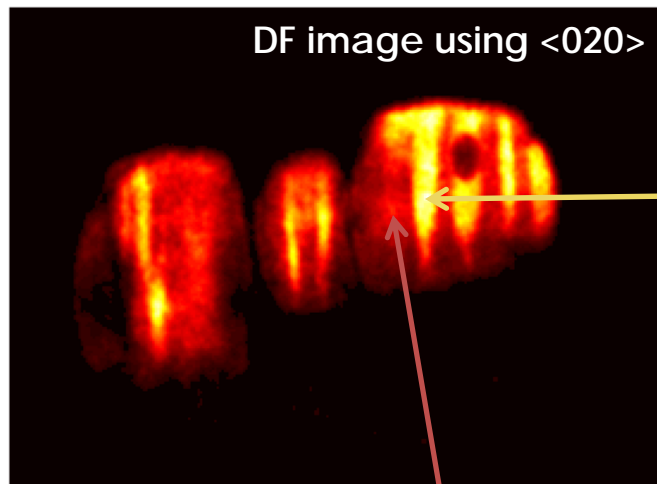
The interfacial energy, γ , between the α -iron matrix and NiAl precipitates is estimated to be $\sim 237 \text{ mJ/m}^2$.

NiAl/Ni₂TiAl-Strengthened Ferritic Superalloys

Fe-2 ~ 6Ti-6.5Al-10Cr-10Ni-3.4Mo-0.25Zr-0.005B (wt. %)

5.1 TEM Microstructural Characterization on Heat-treated Samples

Fe-**2**Ti-6.5Al-10Cr-10Ni-3.4Mo-0.25Zr-0.005B (wt. %), heat-treated sample



- Confirmation of B2-NiAl formation within L2₁-Ni₂TiAl parent precipitate

B2-NiAl zones

L2₁-Ni₂TiAl
parent precipitate

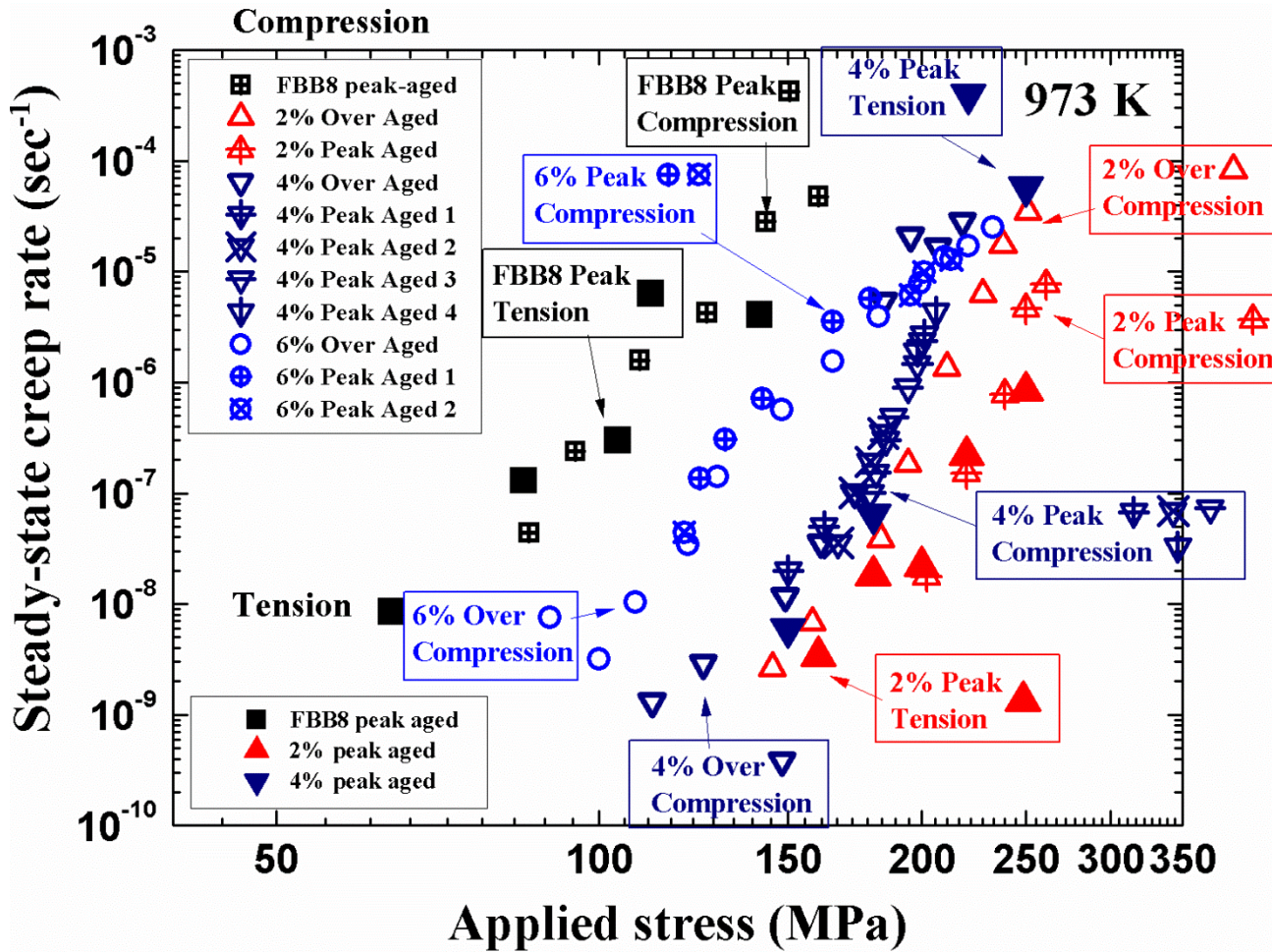
5.2 Creep behaviors

Materials

Fe-6.5Al-10Cr-10Ni-xTi-3.4Mo-0.25Zr-0.005B (wt.%) where $x = 0, 2, 4, \text{ and } 6$

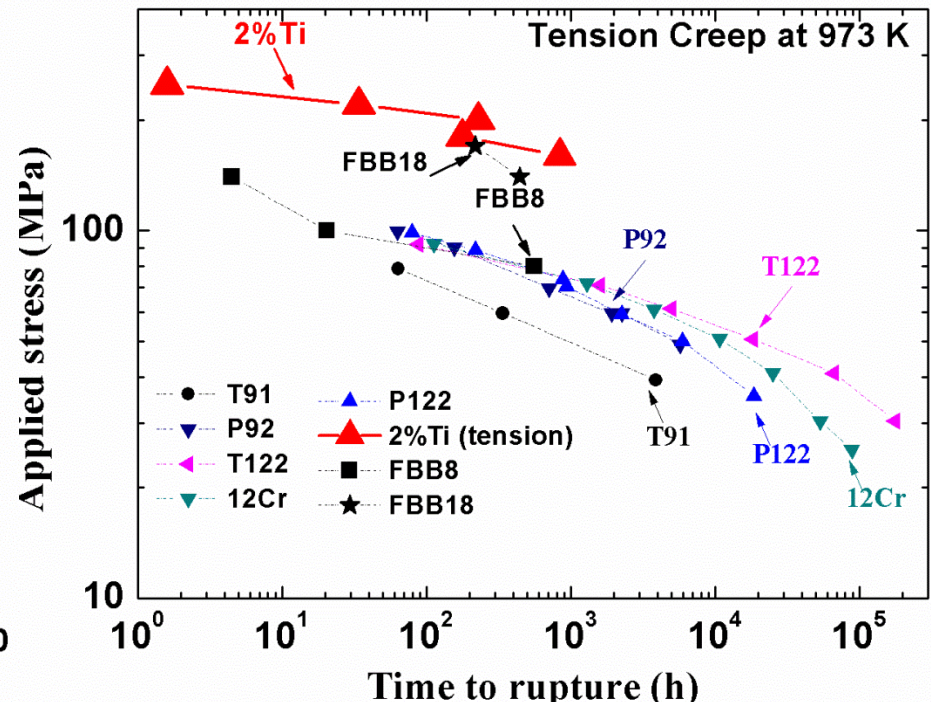
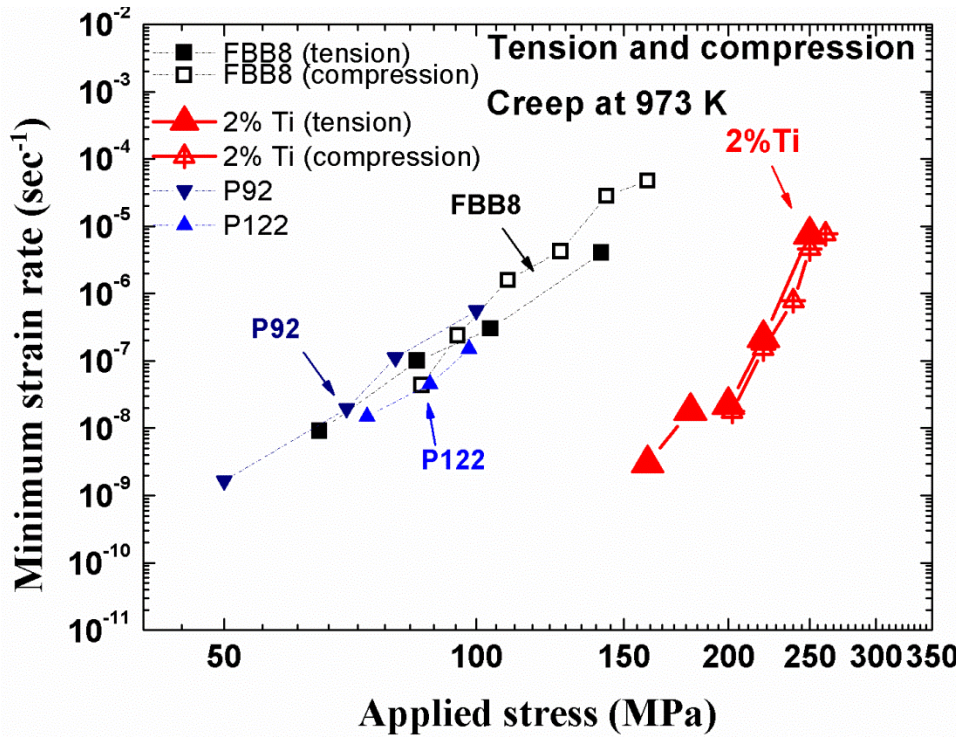
Homogenized at 1200 °C for 0.5, then:

- Peak-aged: 700 °C for 100 h
- Over-aged: 700 °C for 800 h under stress range from 70–270 MPa



5.2 Creep behaviors

Compare with commercial heat-resistant steels:



K. Sawada, K. Kubo, F. Abe, Materials Science and Engineering: A, 319–321 (2001) 784-787.

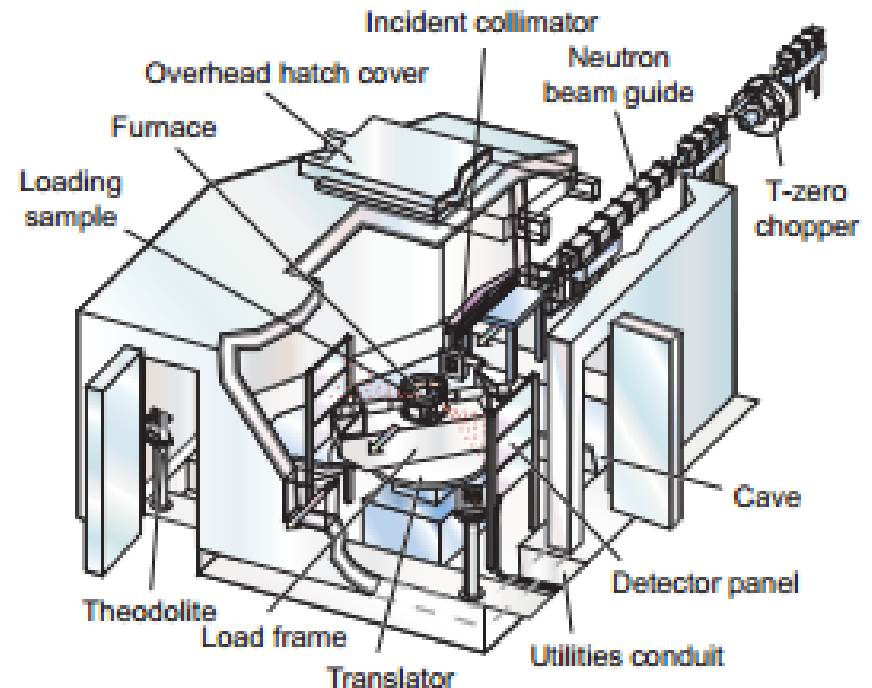
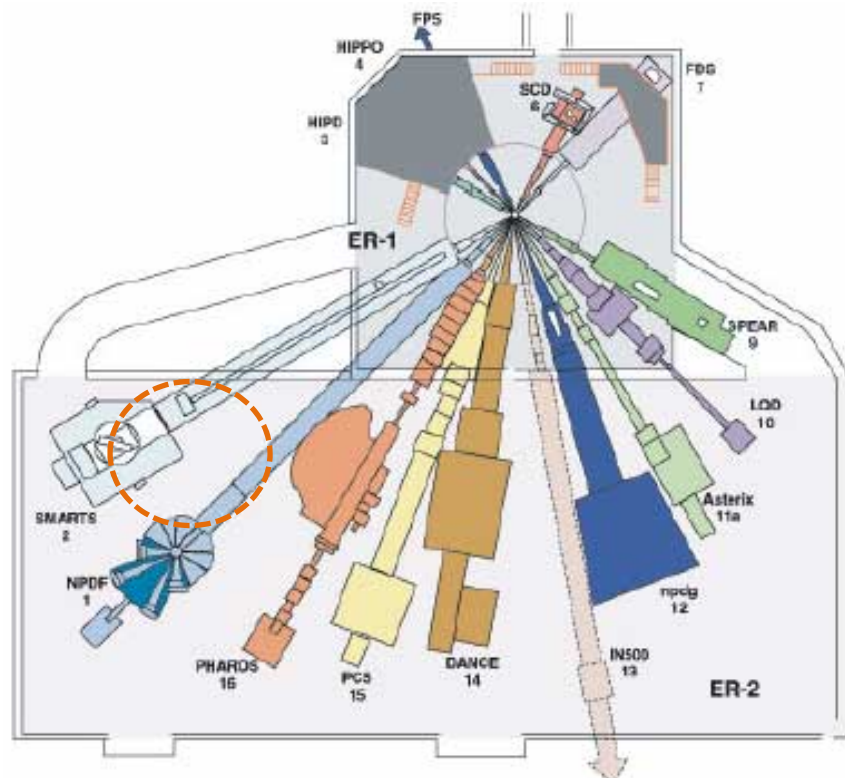
F. Masuyama, N. Komai, Key Engineering Materials, 171 (1999) 179-188.

M. Rieth, A. Falkenstein, P. Graf, S. Heger, U. Jäntschi, M. Klimiankou, E. Materna-Morris, H. Zimmermann, (2004).

S. Latha, M. Mathew, P. Parameswaran, K. Bhanu Sankara Rao, S. Mannan, International Journal of Pressure Vessels and Piping, 85 (2008) 866-870.

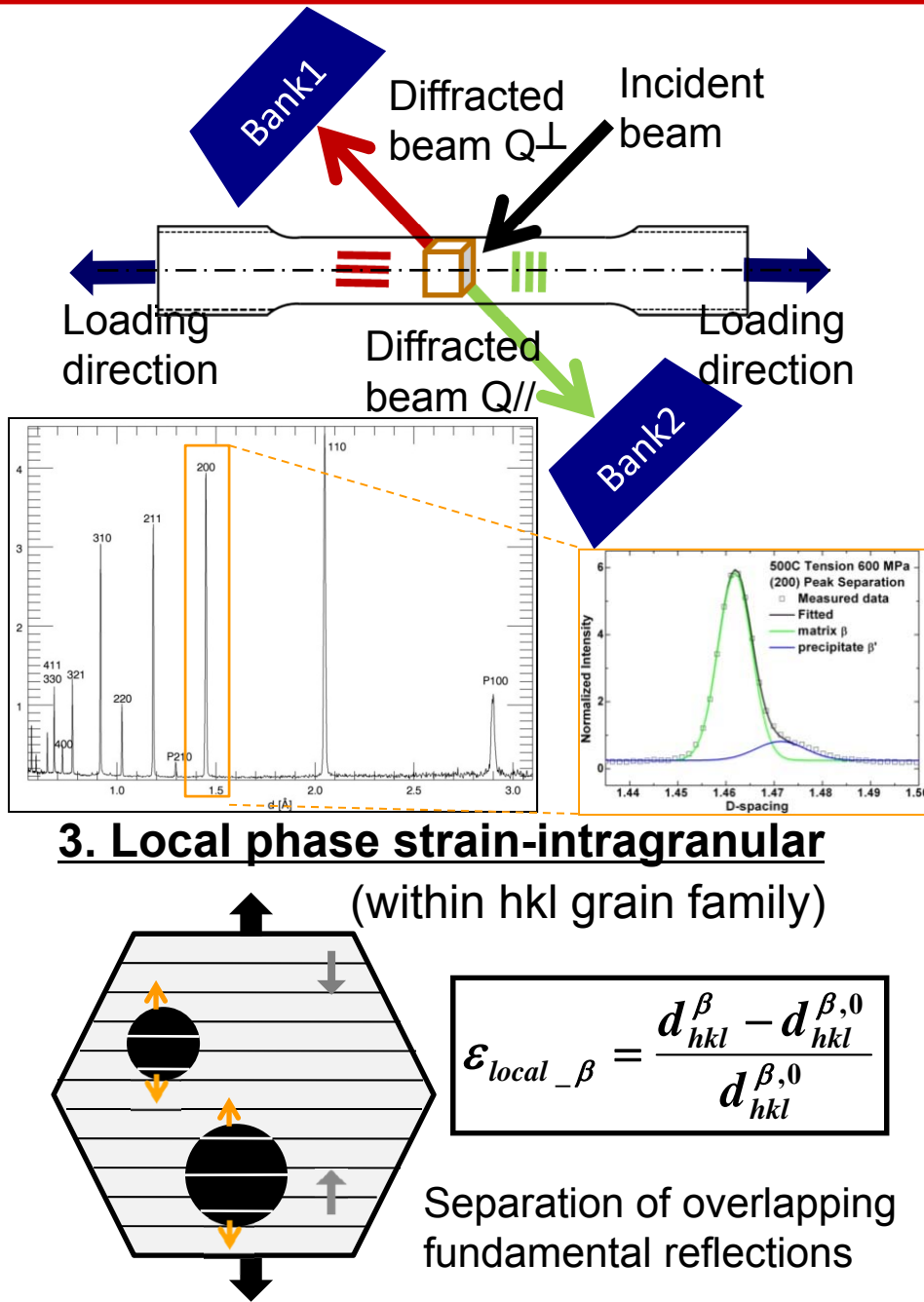
5.3 In-Situ Neutron Creep Studies

Fe-**2Ti-6.5Al-10Cr-10Ni-3.4Mo-0.25Zr-0.005B**

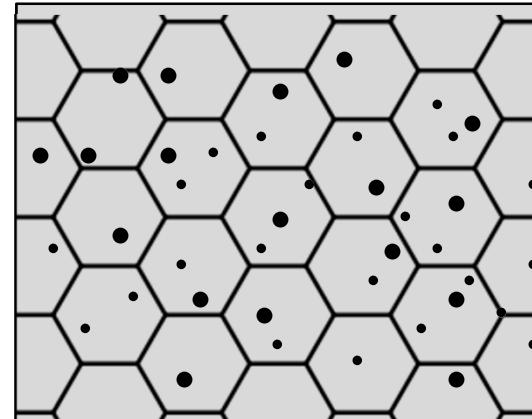


- The experiment was performed at the Spectrometer for Materials Research at Temperature and Stress (SMARTS) located at the Los Alamos Neutron Science Center of the Los Alamos National Laboratory.
- The vacuum furnace and load frame suite at SMARTS allows research on materials under an extreme load (250 kN) and at extreme temperatures (1,550 °C).

5.3 In-situ Neutron Creep Studies



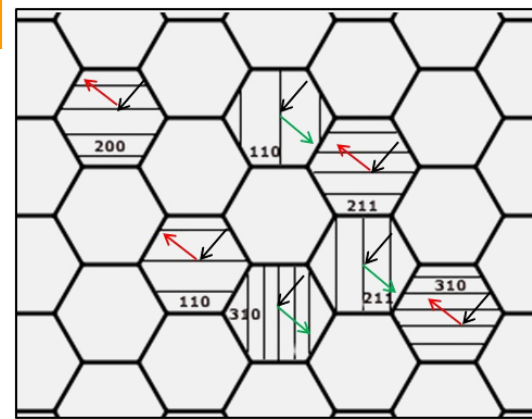
1. Volume-averaged phase strain



$$\varepsilon_{avg_phase} = \frac{a - a_0}{a_0}$$

Rietveld
whole-pattern
fitting

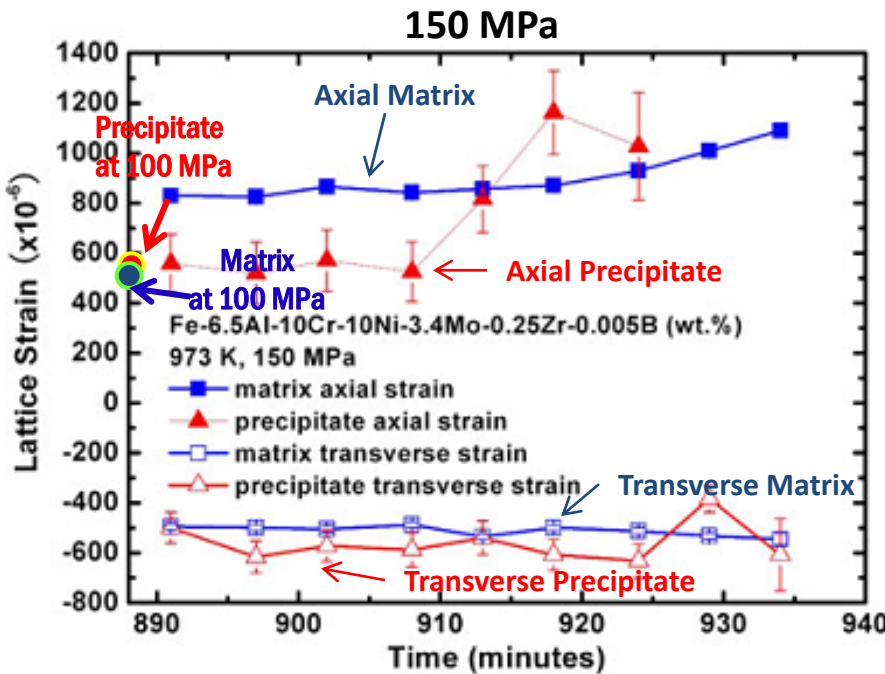
2. hkl-plane specific strain-intergranular



$$\varepsilon_{hkl} = \frac{d_{hkl} - d_{hkl}^0}{d_{hkl}^0}$$

single peak fitting
of overlapping
composite peak

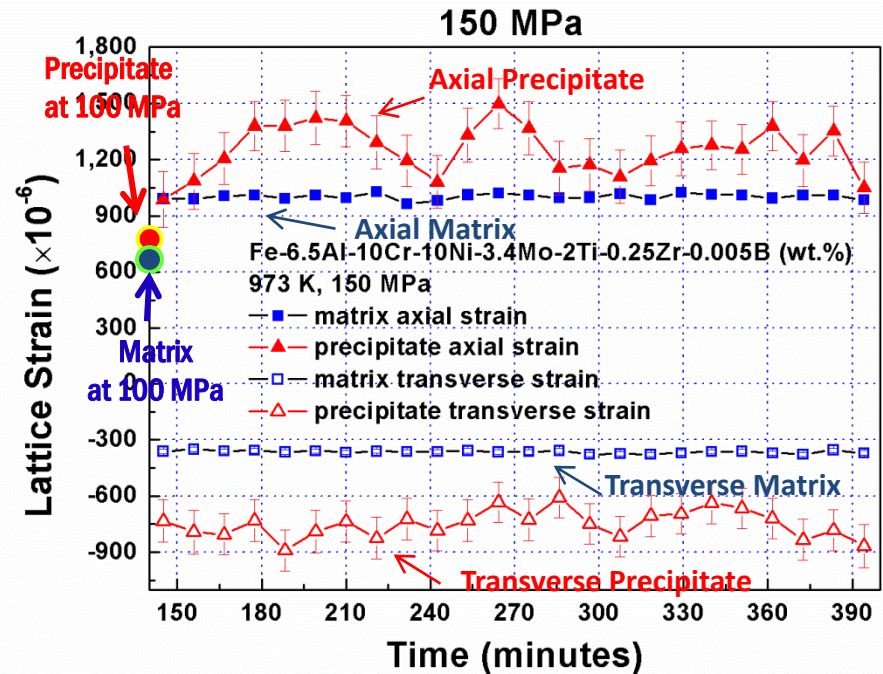
5.3 In-Situ Neutron Creep Studies



NiAl strengthened FBB8

S. Huang, D. W. Brown, B. Clausen, Z. Teng, Y. Gao, and P. K. Liaw, Metallurgical and Materials Transactions A 43: 1497

- The elastic strain of the **precipitate** (about 550μ) at **150 MPa** is more or less **identical** to that at **100 MPa**.
- The elastic strain of the **matrix** at **150 MPa** is raised to 800μ from 600μ at **100 MPa**.

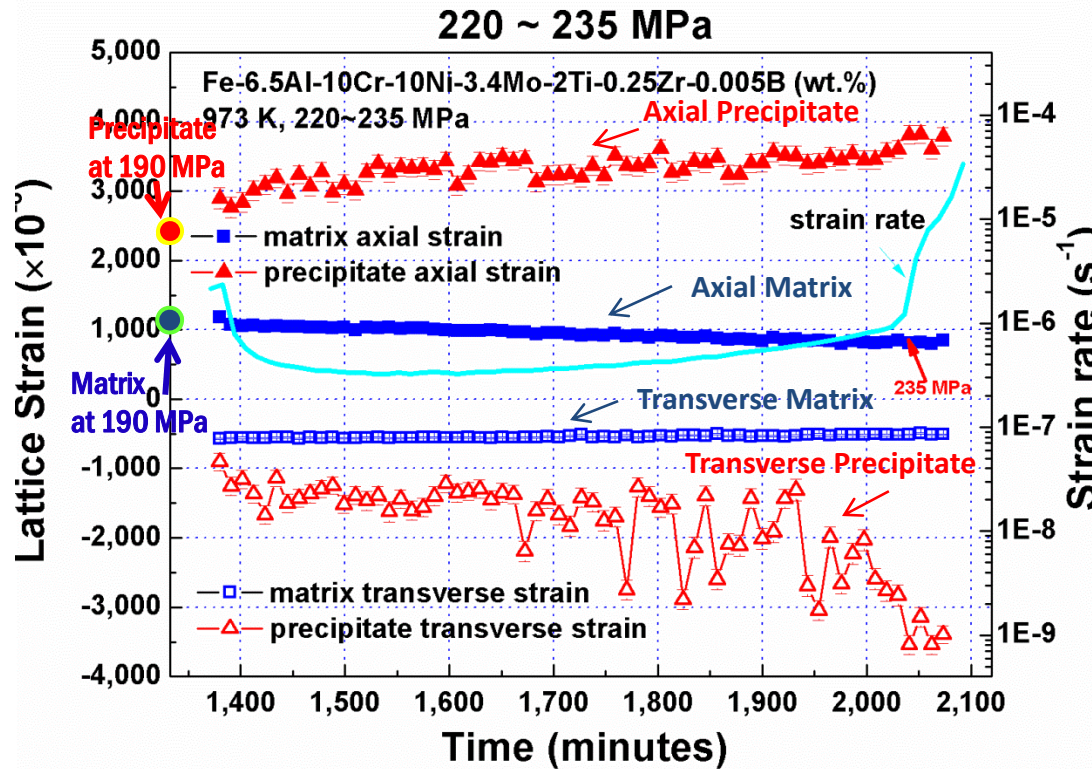


Fe-2Ti-6.5Al-10Cr-10Ni-3.4Mo-0.25Zr-0.005B

- Constant elastic strains for both phases
- The elastic strain of the **precipitate** at **150 MPa** is raised to $1,290 \mu$ from 840μ at **100 MPa**.
- The elastic strain of the **matrix** at **150 MPa** is raised to $1,000 \mu$ from 650μ at **100 MPa**.

NiAl precipitate shows limited load transfer at 973 K, but L_2 -Ni₂TiAl effectively carry more load at 973 K

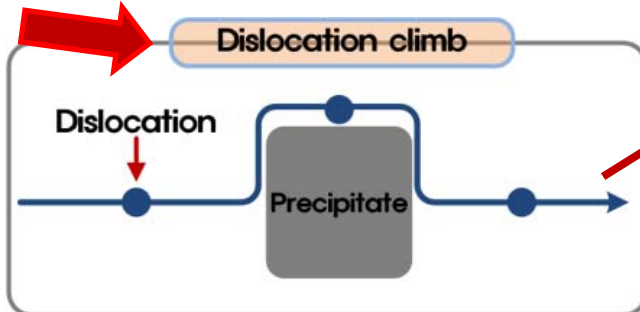
5.3 In-Situ Neutron Creep Studies



- Mainly secondary at 220 MPa, then turn into tertiary region at 235 MPa
- Initial elastic strains ($1,178 \mu$ and 573μ) for the matrix in both directions after the load increase, do not increase as compared to those ($1,144 \mu$ and 526μ) at 190 MPa → indication of **yielding of the matrix for both directions**.
- In both directions, elastic strain for the matrix gradually decreases, whereas that for the precipitate steadily increases → **load transfer from the matrix to precipitate**.

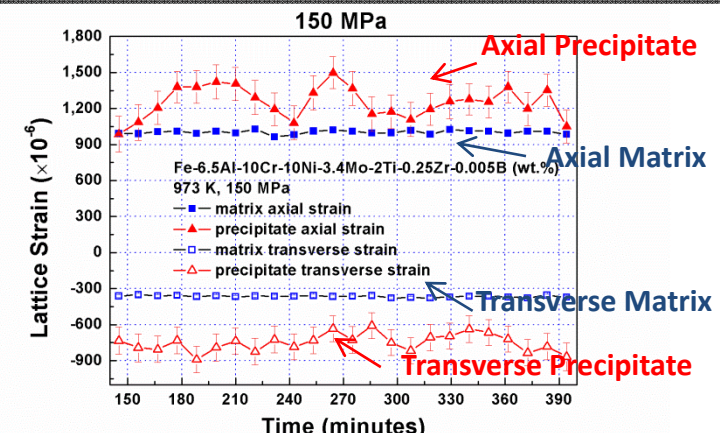
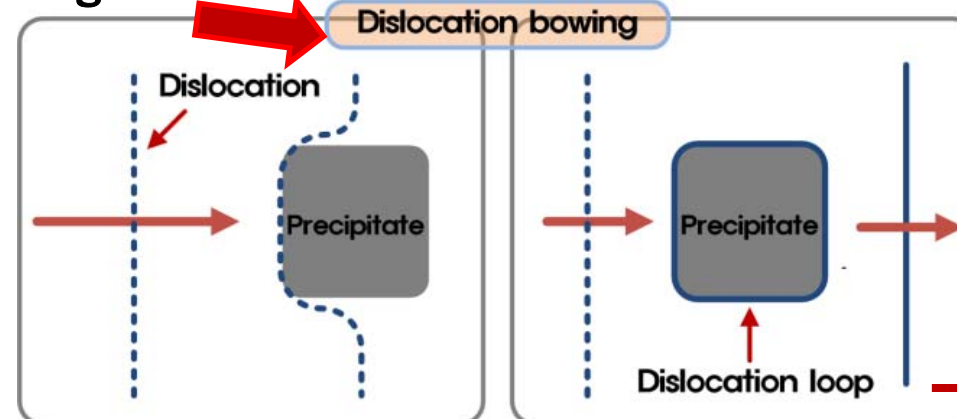
5.3 In-Situ Neutron Creep Studies

At low stresses

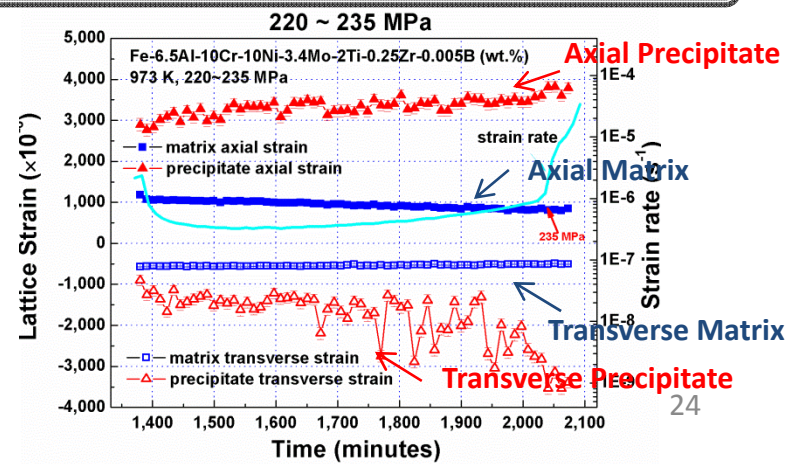
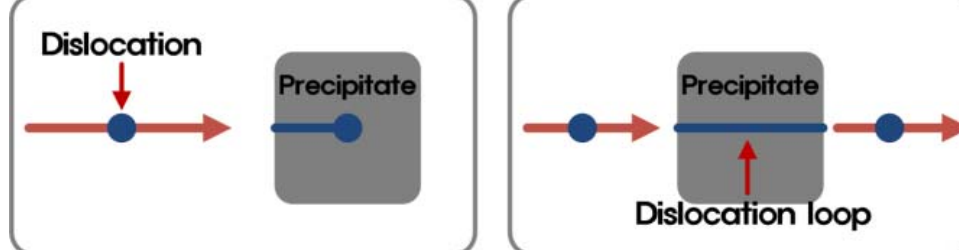


No accumulated dislocation around the precipitate
→ Constant elastic strain of the precipitate (No strong load transfer)

At high stresses



Accumulated dislocations imposing more load to the precipitate
→ Gradual increase in the elastic strain of the precipitate (strong load transfer)



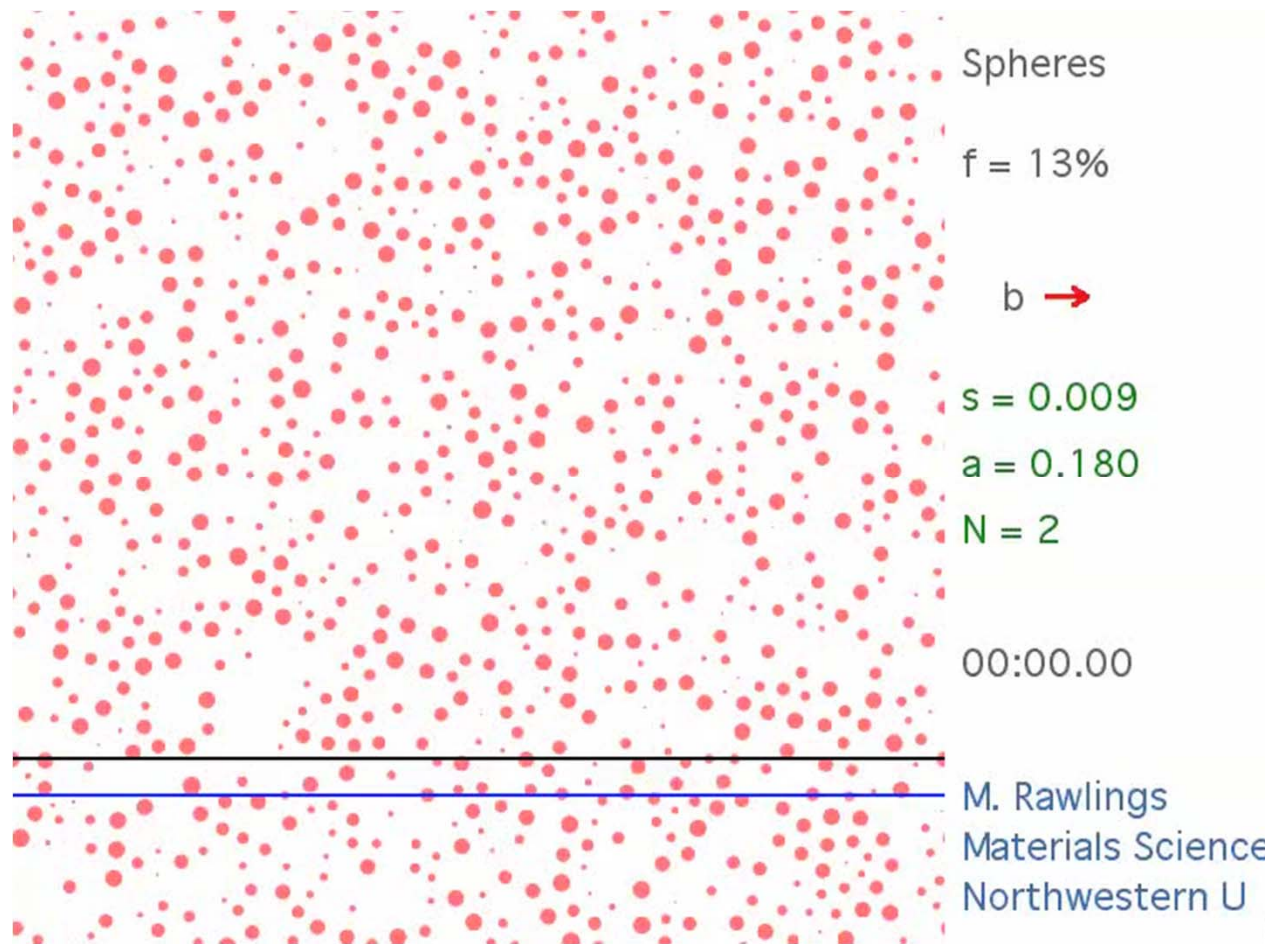
6 Dislocation-Dynamics Simulations

Materials

•Fe-6.5Al-10Cr-10Ni-3.4Mo-0.25Zr-0.005B (wt.%)

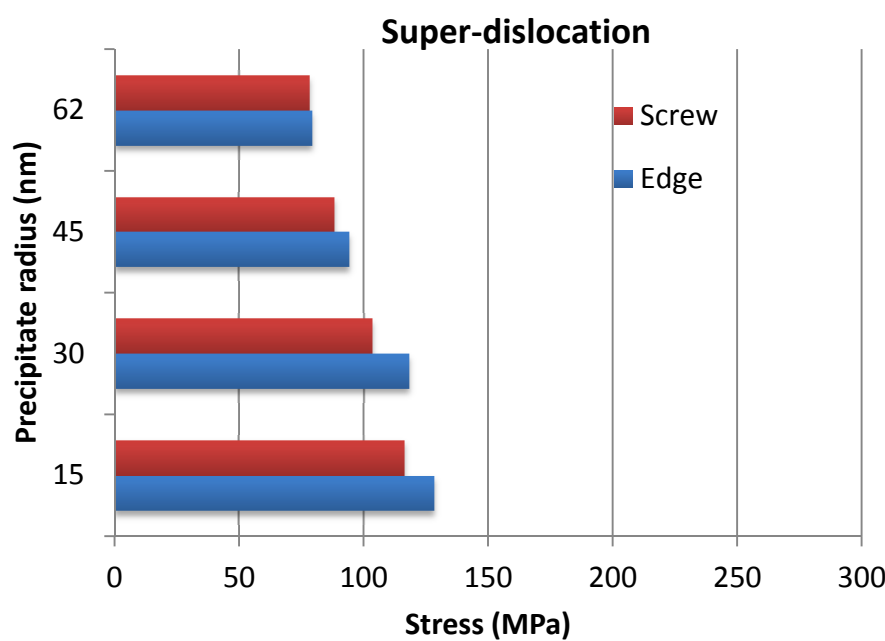
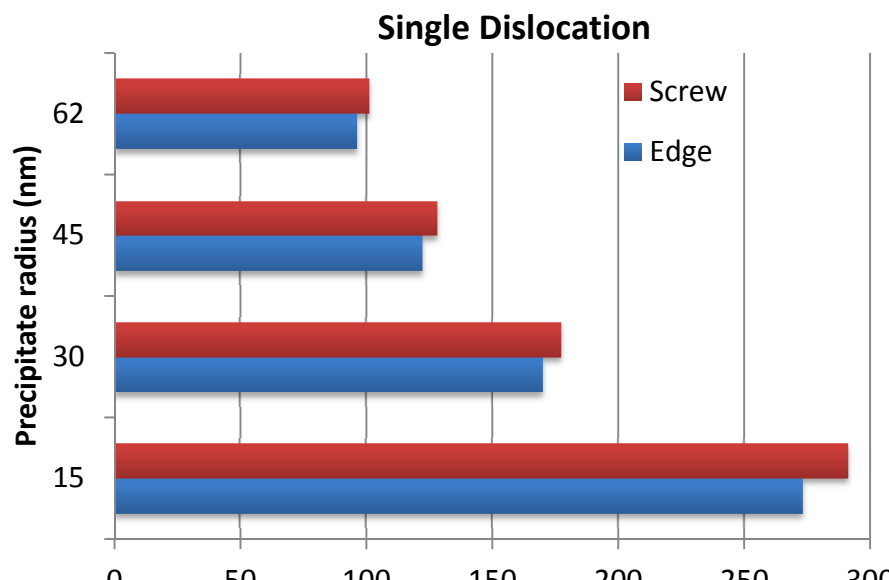
The simulation parameters

- Volume fraction = 13%
- Average radius = 15 nm



Courtesy: Northwestern Univ., unpublished

6 Dislocation-Dynamics Simulations



The simulation parameters:

- Material: Fe-6.5Al-10Cr-10Ni-3.4Mo-0.25Zr-0.005B (wt.%)
- Volume fraction = 13% (Actual Value)

□ Trends:

- Stresses for the single dislocation simulations are significantly higher than in the super-dislocation case for the same conditions
- Values for edge < screw for single dislocation; edge > screw for super-dislocation

□ Yield stress increase experimentally estimated as 79 - 101 MPa for $\langle r \rangle = 62\text{nm}$ (Actual Microstructure)

Papers and Presentations

Papers

- 1) Z. K. Teng, M. K. Miller, G. Ghosh, C. T. Liu, S. Huang, K. F. Russel, M. E. Fine, and P. K. Liaw, *Scripta Materialia*, 2010;63:61.
- 2) S. Huang, D. L. Worthington, M. Asta, V. Ozolins, G. Ghosh, and P. K. Liaw, *Acta Materialia*, 2010;58:1982.
- 3) S. Huang, B. Clausen, D. Brown, Z. K. Teng, Y. F. Gao, and P. K. Liaw, *Metallurgical and Materials Transactions A*, 2012;43:1497.
- 4) Z. K. Teng, F. Zhang, M. K. Miller, C. T. Liu, S. Huang, Y. T. Chou, R. H. Tien, Y. A. Chang, and P. K. Liaw, *Materials Letters*, 2012;71:36.
- 5) Z. K. Teng, G. Ghosh, M. K. Miller, S. Huang, B. Clausen, D. W. Brown, and P. K. Liaw. *Acta Mater.* 2012;60:5362.
- 6) Z. K. Teng, C. T. Liu, M. K. Miller, G. Ghosh, E. A. Kenik, S. Huang, and P. K. Liaw, *Materials Science and Engineering A*, 2012;541:22.
- 7) H. Ding, S. Huang, G. Ghosh, P. K. Liaw, and M. Asta, *Scripta Mater.* 2012;67:732.
- 8) S. Huang, G. Ghosh, X. Li, J. Ilavsky, Z. K. Teng, and P. K. Liaw, *Metallurgical and Materials Transactions A*. 2012;43:3423.
- 9) C. H. Liebscher, V. Radmilovic, U. Dahmen, M. Asta, and G. Ghosh, *Journal of Materials Science*, 2013;48:2067.
- 10) Z. Sun, C. H. Liebscher, S. Huang, Z. Teng, G. Song, G. Wang, M. Asta, M. Rawlings, M. E. Fine, and P. K. Liaw, *Scripta Materialia*, 2013;68:384.
- 11) H. Ding, V. I. Razumovsky, and M. Asta, *Acta Materialia*, 2014;70:130.
- 12) N.Q. Vo, C.H. Liebscher, M.J.S. Rawlings, M. Asta, and D.C. Dunand, *Acta Materialia*, 2014;71:89.

Papers and Presentations

Presentations

- 1) Z. K. Teng, F. Zhang, M. K. Miller, C. T. Liu, A. Y. Chuang, S. Y. Huang, R. H. Tien, Y. T. Chou, and P. K. Liaw. 2011 TMS Meeting, San Diego, 02/27 -03/04.
- 2) S. Y. Huang, B. Clausen, D. Brown, Z. Teng, G. Ghosh, M. Fine, and P. K. Liaw, 2011 TMS Meeting, San Diego, 02/27 -03/04.
- 3) P. K. Liaw, Z. Teng, S. Huang, C. T. Liu, M. E. Fine, G. Ghosh, M. D. Asta, and G. Wang, The Annual University Coal Research/Historically Black Colleges and Universities and Other Minority Institutions Conference, Pittsburgh, PA, 06/07 – 06/08, 2011.
- 4) S. Huang, Y. F. Gao, K. An, W. Wu, L. Zheng, M. Rawlings, D. Dunand, and P. K. Liaw, TMS 141th Annual Meeting, Orlando, FL, Mar., 2012, 03/11 - 03/15.
- 5) P. K. Liaw, M. D. Asta, D. C. Dunand, M. E. Fine, G. Ghosh, and C. T. Liu, National Energy Technology Laboratory, Pittsburgh, 04/18, 2012.
- 6) C. H. Liebscher, V. Radmilovic, U. Dahmen, M. Asta, and G. Gosh, Microscopy & Microanalysis 2012 Meeting, at the Phoenix Convention Center in downtown Phoenix, AZ., 07/29 - 08/02.
- 7) C. H. Liebscher, V. Radmilovic, U. Dahmen, M. Asta, and G. Gosh, Materials Science and Technology 2012 Meeting, Pittsburgh, Pennsylvania, 08/07 - 08/11.
- 8) H. Ding, S. Huang, G. Ghosh, P. K. Liaw, and M. Asta, Materials Science and Technology 2012 Meeting, Pittsburgh, Pennsylvania, 08/07 - 08/11.
- 9) Z. Sun, G. Song, Z. Teng, G. Ghosh, and P. K. Liaw , 2012 MRS Fall Meeting & Exhibit, Boston, 11/25 – 11/30.
- 10) P. K. Liaw, M. Asta, D, Dunand, M. Fine, G. Ghosh, C. Liu, H. Ding, S. Huang, M. Rawlings, Z. Sun, G. Song, Z. Teng, G. Wang, and C. Liebscher, 2013 TMS Meeting , San Antonio, Texas, 03/03 – 03/07
- 11) Z. Sun, S. Huang, Z. Teng, G. Song, G. Wang, and P. K. Liaw, 2013 TMS Meeting , San Antonio, Texas, 03/03 – 03/09

Conclusions

1. Calculations of Interfacial Energies for Fe, B2, and $L2_1$ Phases

- First-principles calculations of the interfacial energies in BCC-Fe/B2-NiAl, BCC-Fe/ $L2_1$ -Ni₂TiAl, and B2-NiAl/ $L2_1$ -Ni₂TiAl have been carried out.
- The first-principles calculation is a viable option, compared to the time-consuming coarsening study.
- Furthermore, it is well known that the shape evolution in the coherent microstructure is governed by subtle interplay between interfacial and strain energies (relevant to elastic constant calculations).

Conclusions (Cont'd)

2. Coarsening Kinetics of NiAl Precipitates in FBB8

- The coarsening kinetics of NiAl precipitates in FBB8 at 700, 800, and 950 °C has been investigated.
- It satisfies the linear relationship between \bar{r} and $t^{1/3}$. The coarsening rates are 13, 38, and 143 nm/h^{1/3} at 700, 800, and 950 °C, respectively.
- The interfacial energy between the α-iron matrix and NiAl precipitates is estimated to be ~ 237 mJ/m², which is comparable to the value calculated by first principles.

Conclusions (Cont'd)

3. NiAl/Ni₂TiAl-Strengthened Ferritic Superalloys

- TEM shows the formation of an NiAl phase in the Ni₂TiAl parent precipitate for the 2% Ti-containing alloy.
- Systematic creep tests have been performed on FBB8-based new alloys at 973 K. These Ti-containing alloys, especially the 2% Ti alloy, have superior creep resistance, compared to commercial heat-resistant ferritic steels and NiAl-strengthened ferritic alloys.

4. In-Situ Neutron Creep on the 2% Ti alloy

- The in-situ neutron creep test on the 2% Ti alloy at 973 K was performed using SMARTS located at the Los Alamos National Laboratory.
- The evolution of the elastic strain shows the dependence of the creep-deformation mechanisms, such as dislocation climb and bowing.

Conclusions (Cont'd)

5. Dislocation-Dynamics Simulations

- The dislocation-dynamics simulations have been performed in order to understand the strengthening effect of precipitates.

6. Future Work

- Systematic creep experiments at different temperatures and stresses and complementary TEM will be conducted to understand the creep mechanisms.
- Creep-deformation behavior will be simulated by dislocation dynamics to develop mechanistic models and predict creep-deformation characteristics.

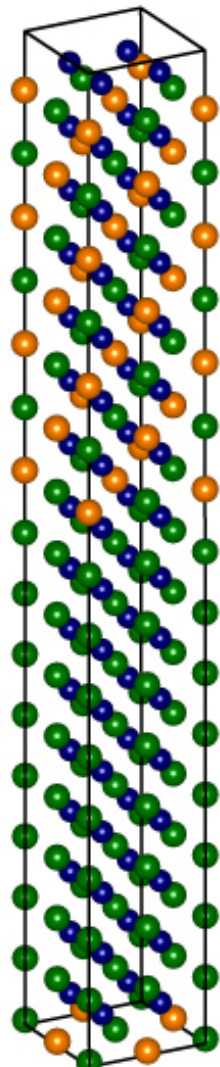
Q & A

Thank you for your kind
attention

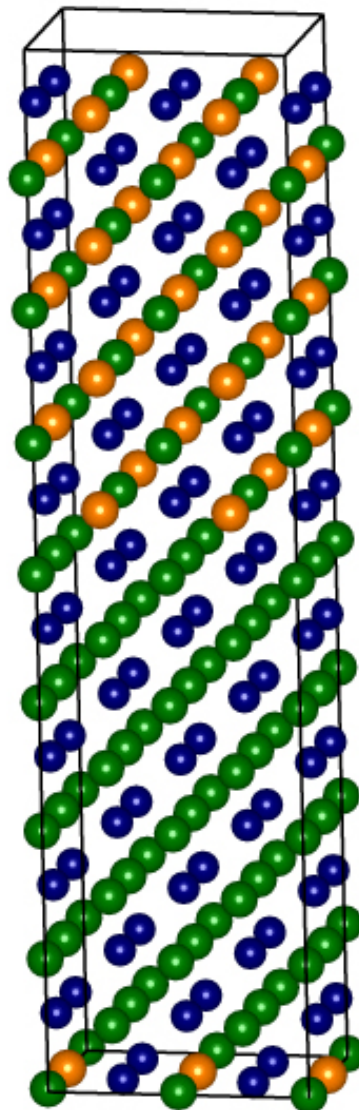
3 Calculations of Interfacial Energies for Fe, *B2*, and *L2₁* Phases

Atomic scale structural models of $B2\text{-NiAl}/L2_1\text{-Ni}_2\text{TiAl}$ with a coherent interface:

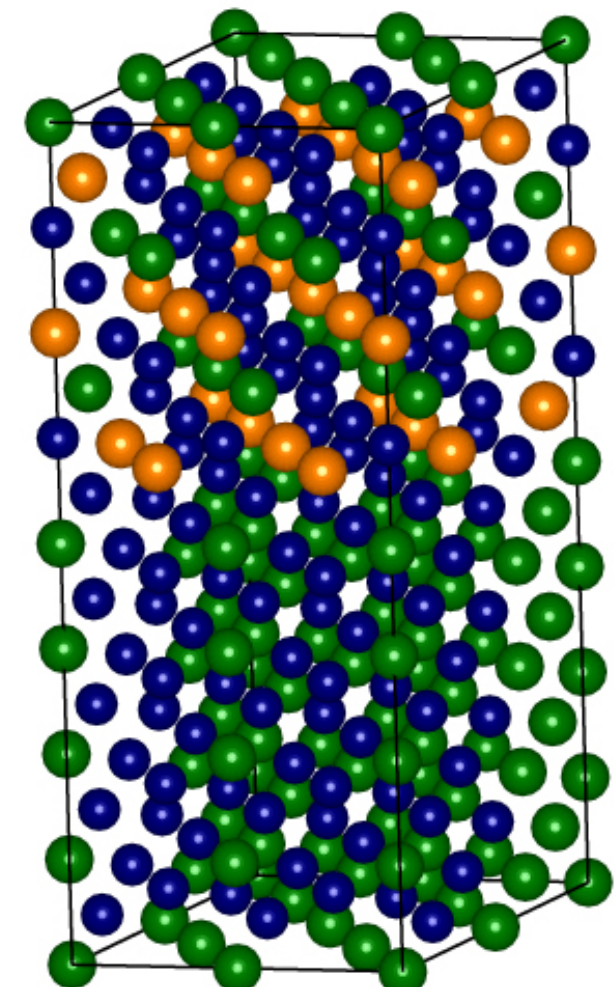
(100) habit



(110) habit



(111) habit



green: Ni, blue: Al, yellow: Ti

5.2 Creep behaviors

□ The creep strain rate

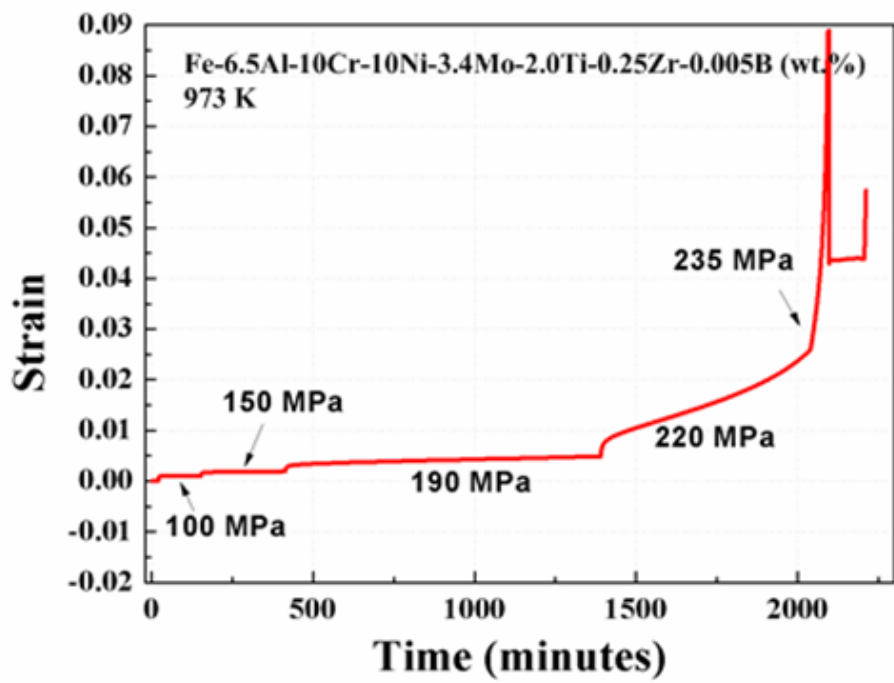
$$\dot{\varepsilon}_s = A \frac{GbD}{kT} \left(\frac{\sigma - \sigma_{th}}{G} \right)^n$$

A: Constant; D: Effective diffusion coefficient; k: Boltzmann constant; T: Temperature; σ : Applied stress; σ_{th} : Threshold stress; n: creep-stress exponent of the matrix without particles.

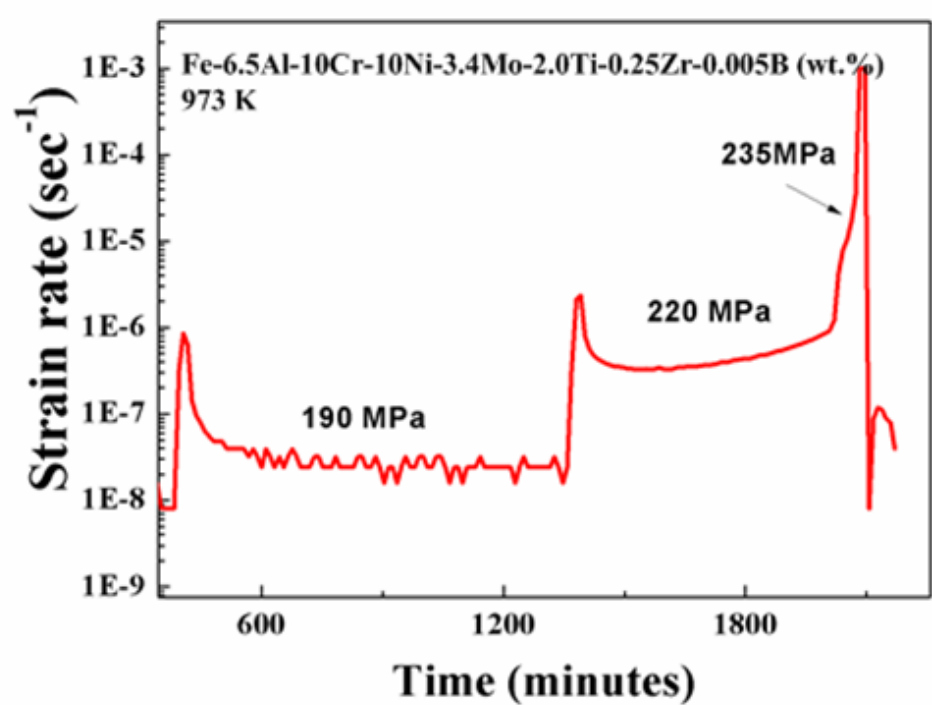
Samples Tested	Threshold Stress (MPa)
FBB8 Peak-aged	70 ± 1
FBB8+6% Ti Over-aged	87 ± 1
FBB8+6% Ti Peak-aged	90 ± 1
FBB8+4% Ti Over-aged	144 ± 35
FBB8+4% Ti Peak-aged	129 ± 43
FBB8+2% Ti Over-aged	172 ± 1
FBB8+2% Ti Peak-aged	179 ± 1

5.3 In-Situ Neutron Creep Studies

Strain vs. Time



Strain rate vs. Time



- The sample was subjected to constant loads of 100, 150, 190, 220, and 235 MPa for various periods. The diffracted neutron signal in the axial and transverse directions was continuously collected.
- The total measuring time is ~ 33 h, and the final rupture strain ~ 9%.

Future Work

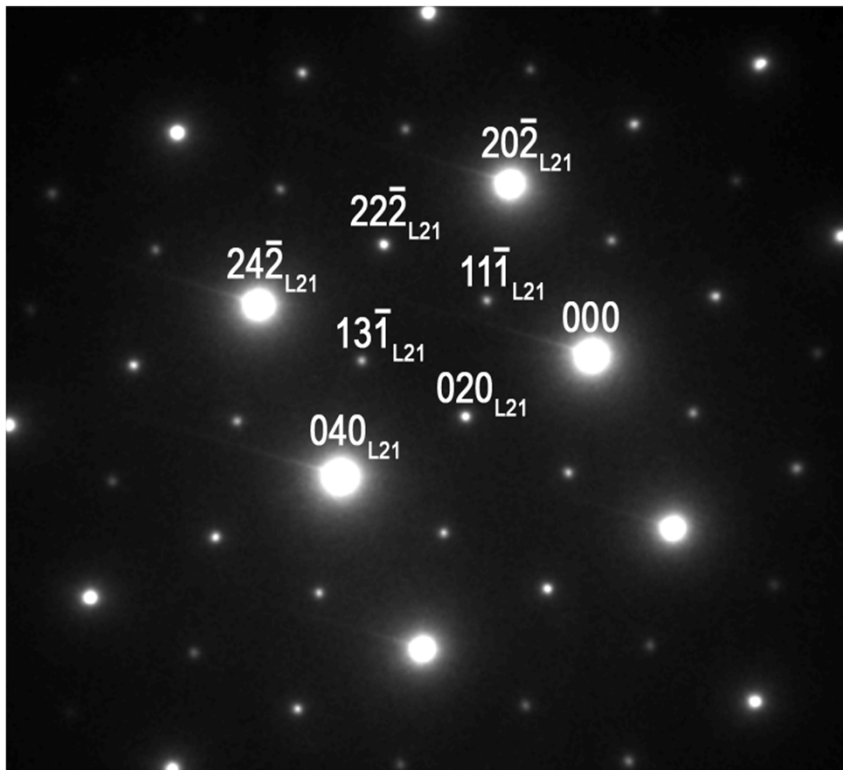
Understanding of creep mechanisms on 2% Ti alloy

1. Systematic creep experiments will be conducted at different temperatures and applied stresses to obtain all crucial creep parameters, including stress exponents, activation energies, and threshold stresses.
2. A complementary transmission electron microscope (TEM) study on crept specimens of the 2% Ti alloy will be carried out in order to examine the detailed interactions between dislocations and precipitates.
3. In-situ neutron creep data will be analyzed using single-peak fitting to understand the inter-granular interaction between differently-oriented grains during creep deformation.
4. With the experimental results, including TEM, creep, and in-situ neutron creep, creep-deformation will be predicted by dislocation-dynamics simulations, which enable us to develop mechanistic models and predict creep-deformation behaviors.

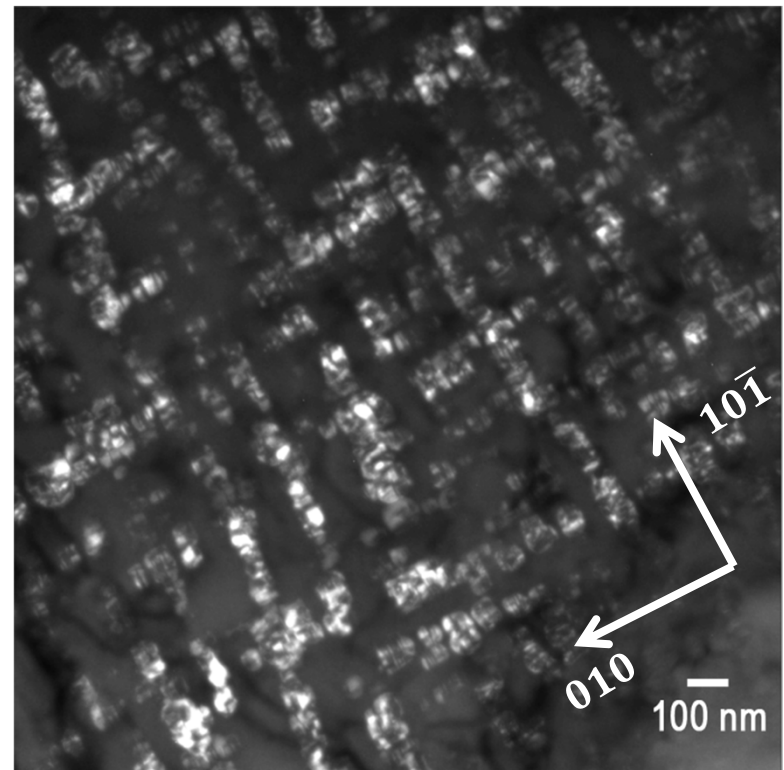
5.1 TEM Microstructural Characterization on Heat-treated Samples

Fe-**2Ti**-6.5Al-10Cr-10Ni-3.4Mo-0.25Zr-0.005B (weight percent), heat-treated sample

<101> zone-axis diffraction pattern



Dark-field (DF) image using <111>



- Clear indication of L2₁-type reflections:
 - <111> and <131> unique to L2₁-Ni₂TiAl
 - <020> and <222> common to both B2-NiAl and L2₁-Ni₂TiAl

- Cuboidal, elongated L2₁-type (Ni₂TiAl) precipitates, width ~ 50 – 80 nm
- Cube-on-orientation of bcc-Fe matrix and L2₁-type precipitates
→ indication that <100> elastically softest direction